Ferroelectric-like Behavior Originating from Oxygen Vacancy Dipoles in Amorphous Film for Non-volatile Memory

Yue Peng[1], Genquan Han[1*], Fenning Liu[1], Wenwu Xiao[1], Yan Liu[1], Ni Zhong[2], Chungang Duan[2], Ze Feng[3], Hong Dong[3] and Yue Hao[1]

Abstract

Traditional ferroelectric devices suffer a lack of scalability. Doped HfO_2 thin film is promising to solve the scaling problem but challenged by high leakage current and uniformity concern by the polycrystalline nature. Stable ferroelectric-like behavior is firstly demonstrated in a 3.6-nm-thick amorphous Al_2O_3 film. The amorphous Al_2O_3 devices are highly scalable, which enable multi-gate non-volatile field-effect transistor (NVFET) with nanometer-scale fin pitch. It also possesses the advantages of low process temperature, high frequency (~GHz), wide memory window, and long endurance, suggesting great potential in VLSI systems. The switchable polarization (P) induced by the voltage-modulated oxygen vacancy dipoles is proposed.

Keywords: Amorphous, Al_2O_3, Ferroelectric, Memory, Oxygen vacancy dipole, Non-volatile field-effect transistor

Background

Ferroelectric random access memory (FeRAM) based on conventional perovskite ferroelectrics (e.g., PZT) has been one of the commercial non-volatile memories (NVMs) [1], although it cannot be scaled and not CMOS-compatible. Ferroelectricity was widely observed in a variety of different materials, such as porcine aortic walls [2], Sb_2S_3 nanowires [3], $GaFeO_3$ film [4], doped poly-HfO_2 films [5], nanocrystalline hydroxyapatite films [6], and $LaAlO_3$-$SrTiO_3$ film [7]. Among these materials, doped-HfO_2 films have attracted special interests for the NVM application due to their CMOS process compatibility. But the polycrystalline structure is inevitable to generate ferroelectricity in doped-HfO_2, which brought obstacles for device application to overcome as follows: 1) it is incompatible with the gate-last processing with regard to the thermal budget of 500 °C required to form orthorhombic crystal phases [8]; 2) power consumption

is induced from undesired leakage current along the grain boundaries, which increases exponentially along with the scaling down of ferroelectric thickness. Recently, a theoretical study proposed that the additional ferroelectricity in thick poly-HfO_2 (>5 nm) can come from the long-range correlations in the assembly of electric dipoles created by oxygen vacancies [9]. The defect charge trapping/detrapping mechanism was observed to produce the ferroelectric-like behavior in a 5-nm-thick amorphous Al_2O_3 for a multi-state memory, which, however, suffers from a very low trapping/detrapping frequency (e.g., ~500 Hz) [10].

In this work, stable ferroelectric-like behavior is demonstrated in a 3.6-nm-thick amorphous Al_2O_3 film, where the switchable polarization (P) is proposed to be induced by the voltage-modulated oxygen vacancy dipoles. The amorphous Al_2O_3 film possesses the advantages of low process temperature and the operating frequency up to ~GHz, which enable multi-gate non-volatile field-effect transistor (NVFET) with nanometer-scale fin pitch. Al_2O_3 NVFET memory with a 100-ns pulse width program/erase (P/E) voltages and over 10^6

* Correspondence: hangenquan@gmail.com; gqhan@xidian.edu.cn
[1]State Key Discipline Laboratory of Wide Band Gap Semiconductor Technology, School of Microelectronics, Xidian University, Xi'an 710071, China
Full list of author information is available at the end of the article

P/E cycles endurance is demonstrated. The effects of electrodes and film thickness on the P in Al_2O_3 capacitors are also investigated. The amorphous non-volatile devices show a promising future in VLSI memories.

Methods

Amorphous Al_2O_3 films were grown on Si(001), Ge(001), and TaN/Si substrates by atomic layer deposition (ALD). TMA and H_2O vapor were used as the precursors of Al and O, respectively. During the deposition, the substrate temperature was maintained at 300 °C. Different top metal electrodes, including TaN/Ti, TaN, and W, were deposited on Al_2O_3 surfaces by reactive sputtering. Capacitors with different electrodes were fabricated by lithography patterning and dry etching. Rapid thermal annealing (RTA) at 350 °C for 30 s was performed. NVFETs with TaN/Al_2O_3 gate stack were fabricated on Ge(001). After gate formation, source/drain (S/D) regions were implanted by BF_2^+ with a dose of 1 × 10^{15} cm^{-2} and an energy of 20 keV, and 20 nm-thick nickel S/D metal electrodes were then formed by lift-off process. Figure 1a and b shows the schematics of the fabricated Al_2O_3 capacitor and the p-channel NVFET. There is an interfacial layer (IL) between the electrode and the Al_2O_3 film. Figure 1c and d show the high-resolution transmission electron microscope (HRTEM) images of the TaN/Al_2O_3/Ge stacks with different amorphous Al_2O_3 thicknesses (t_{AlO}) after an RTA at 350 °C.

Results and Discussion

Figure 2 shows the measured P vs. voltage V characteristics for the amorphous Al_2O_3 capacitors with different t_{AlO} and various top and bottom electrodes. The measurement frequency is 1 kHz. As shown in Fig. 2a–c, with a

fixed 3.6 nm of t_{AlO}, TaN/Al_2O_3/Ge capacitor achieves a higher saturation P (P_{sat}) compared to the devices with TaN/Ti and W top electrodes. The ferroelectric-like behavior is strongly correlated with interfaces, and it is proposed that the formation of TaAlO$_x$ IL between TaN and Al_2O_3 produces more oxygen vacancies, contributing to a stronger switching P, compared to the TiAlO$_x$ and WAlO$_x$ ILs. P-V curves in Fig. 2d indicate that TaN/Al_2O_3/TaN capacitor has a much higher P_{sat} in comparison with TaN/Al_2O_3/Ge, which is attributed to the fact that dual TaAlO$_x$ ILs provide higher oxygen vacancy concentration. While P_{sat} is significantly lower from that with Si bottom electrode (Fig. 2e), compared with the Ge electrode. This result indicates that Al_2O_3/Si interface quality is better, i.e., fewer oxygen vacancies, compared to that from the device based on Ge substrate. Figure 2f shows the P-V curves of a TaN/Al_2O_3(6 nm)/Ge capacitor, exhibiting a higher V_c and an almost identical P_{sat} as compared to that from the device with 3.6 nm of Al_2O_3 film in Fig. 2b. It is noted that the reason for the unclosed P-V loops is because a leakage indeed exists. It was reported that the large offset at an electric field of zero always occurred with a large field, and it always disappeared gradually with the smaller sweeping range of V [11, 12].

Figure 2g and h show the extracted evolution of the positive and negative remnant P (P_r) and coercive V (V_c) values, respectively, over 10^4 sweeping cycles for a TaN/Al_2O_3/Ge capacitor. No wake-up, imprint, or fatigue effect is observed. V_c of the device is ~1.8 V, indicating that the E in the Al_2O_3 film is 4~6 MV/cm and in the ILs can exceed 8 MV/cm, which is high enough to drive the oxygen vacancies [13, 14]. P_{sat} of the devices ranges from 1 to 5 $\mu C/cm^2$, corresponding to a reasonable oxygen vacancy concentration in the range 3~15×10^{12} cm^{-2} assuming they have charge of plus two.

Fig. 1 Schematics of the fabricated **a** Al_2O_3 capacitors with various electrodes and **b** Al_2O_3 NVFET. **c** and **d** HRTEM images of the fabricated TaN/Al_2O_3/Ge stacks with different t_{AlO}, showing the amorphous Al_2O_3 films after an RTA at 350 °C

Peng *et al. Nanoscale Research Letters* (2020) 15:134

Page 3 of 6
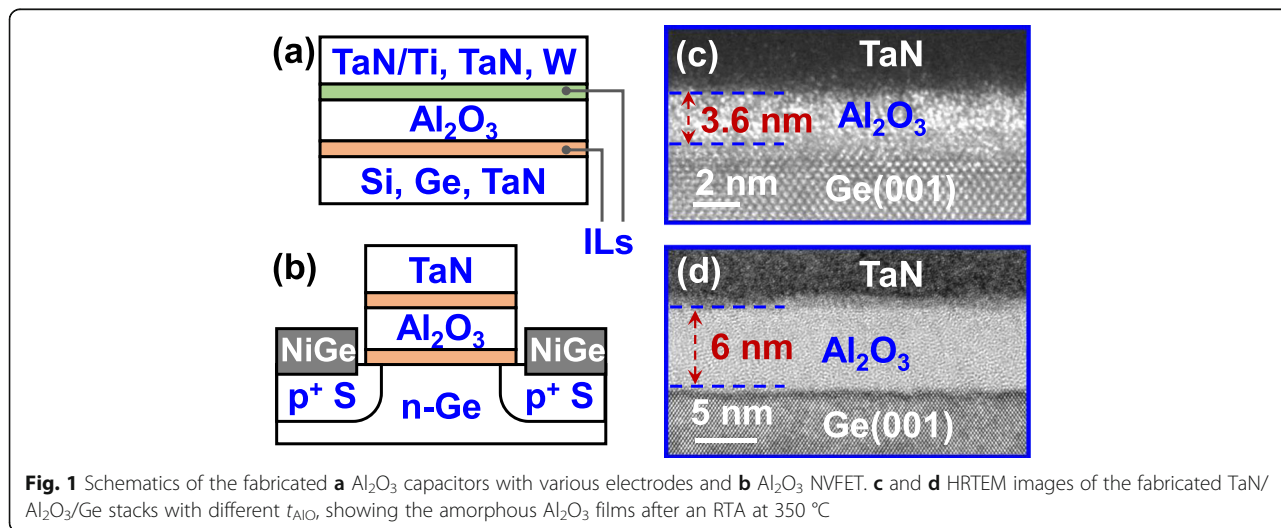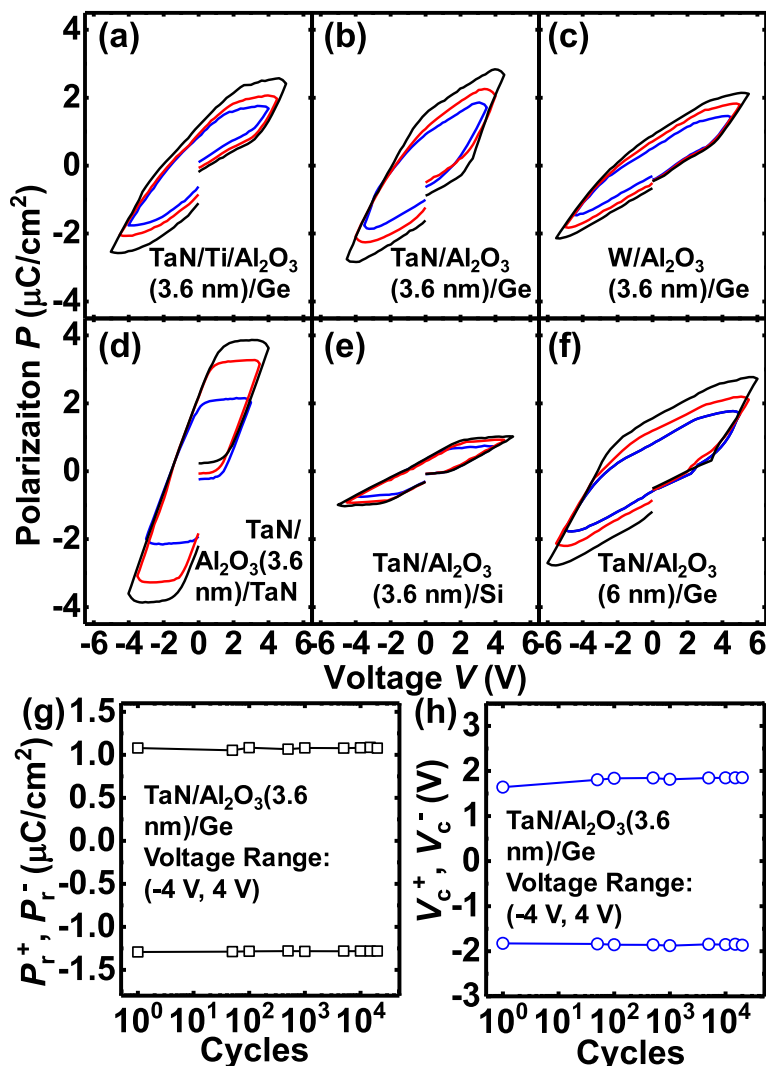
Fig. 2 Measured *P* vs. *V* characteristics of the Al_2O_3 capacitors with different electrodes. **a**, **b**, and **c** showing the *P-V* curves of TaN/Ti/Al_2O_3/Ge, TaN/Al_2O_3/Ge, and W/Al_2O_3/Ge, respectively, with a 3.6-nm t_{AlO}. **d** and **e** showing that the P_{sat} is enhanced(reduced) by using TaN(Si) as the bottom electrode instead of Ge. **f** TaN/Al_2O_3(6 nm)/Ge capacitor has a higher V_c and a similar P_{sat} compared to the 3.6-nm-thick device in **b**. **g** and **h** Endurance measurements showing no degradation of P_r and V_c observed after 10^4 sweeping cycles for a TaN/Al_2O_3(3.6 nm)/Ge capacitor

The underlying mechanism for ferroelectric-like behavior associated with oxygen vacancies in Al_2O_3 devices is discussed. The migration of the voltage-driven oxygen vacancies has been widely demonstrated in resistive random-access memory devices [15, 16]. Figure 3 shows the schematics of the switchable *P* in TaN/Al_2O_3/Ge, which originates from the segregation of voltage-modulated oxygen vacancies and negative charges to form the electrical dipoles. It is reasonable to infer that the movable oxygen vacancies mainly arise from the formation of TaAlO$_x$ IL and are located in the vicinity of the top interface at the initial state (Fig. 3a). Figure 3b and c indicate how the positive and negative *P* are formed, respectively, with the modulation of the oxygen vacancy and negative charge dipoles under the applied

voltage. X-ray photoelectron spectra (XPS) of Al_2O_3/Ge and (Ti, TaN, and W)/Al_2O_3/Ge samples are measured and shown in Fig. 4). For all the metal/Al_2O_3/Ge samples, there is a metal oxide IL formed between metal and Al_2O_3, which are proposed to be the reservoir of oxygen ions and vacancies, which is consistent with Ref. [17].

To characterize the electrical performance of Al_2O_3 NVFET as NVM, program (erase) operation is achieved by applying positive (negative) voltage pulses to the gate, to raise (lower) its threshold voltage (V_{TH}). Figure 5a shows how the linear-region transfer characteristics of the Al_2O_3 NVFET shift relative to the initial I_{DS}-V_{GS} curve measured with ±4 V program (erase) voltages with 100 ns pulse width. Here, V_{TH} is defined as a V_{GS} at 100 nA·W/L, and MW is defined as the maximum change in
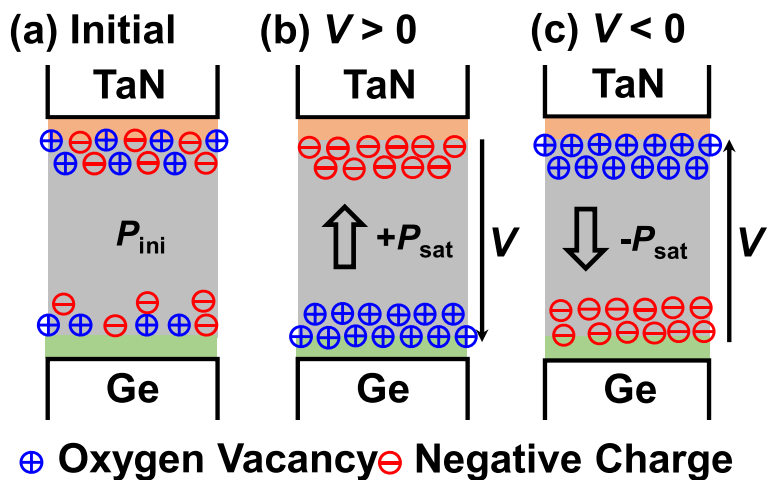
Fig. 3 Schematics of the mechanism for ferroelectric-like behavior in Al_2O_3 capacitors. Switchable P is due to the migration of oxygen vacancies and negative charges to form dipoles
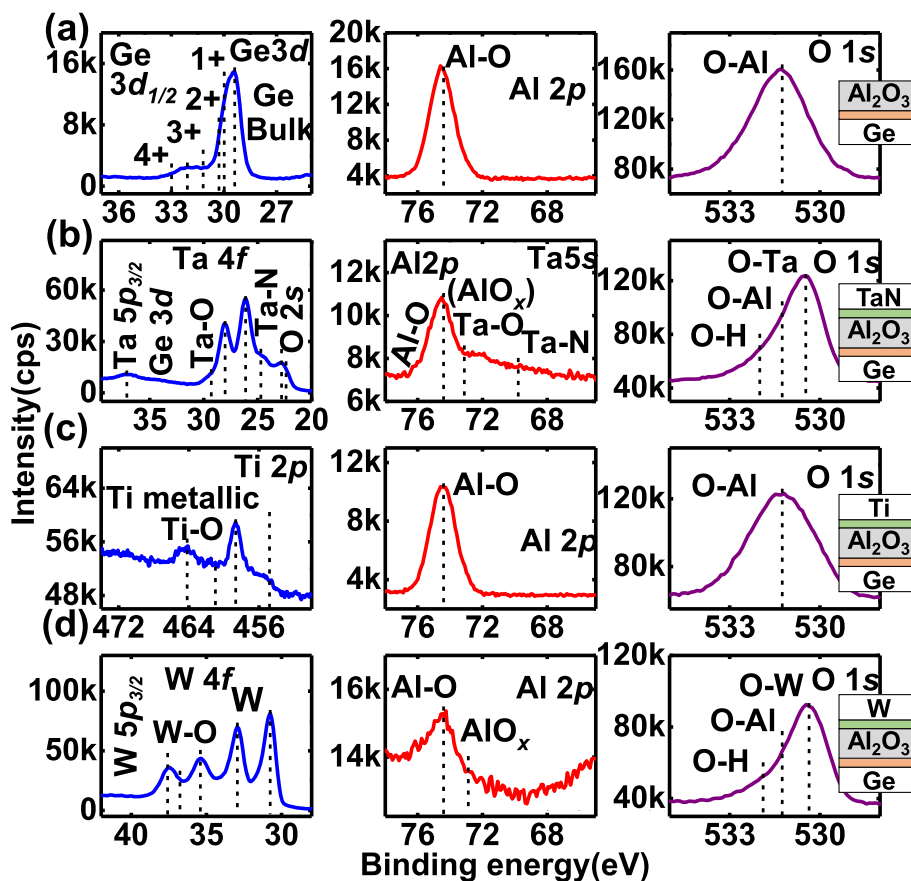
Fig. 4 Core level XPS spectra of **a** Al_2O_3/Ge, **b** TaN/Al_2O_3/Ge, **c** Ti/Al_2O_3/Ge, and **d** W/Al_2O_3/Ge samples
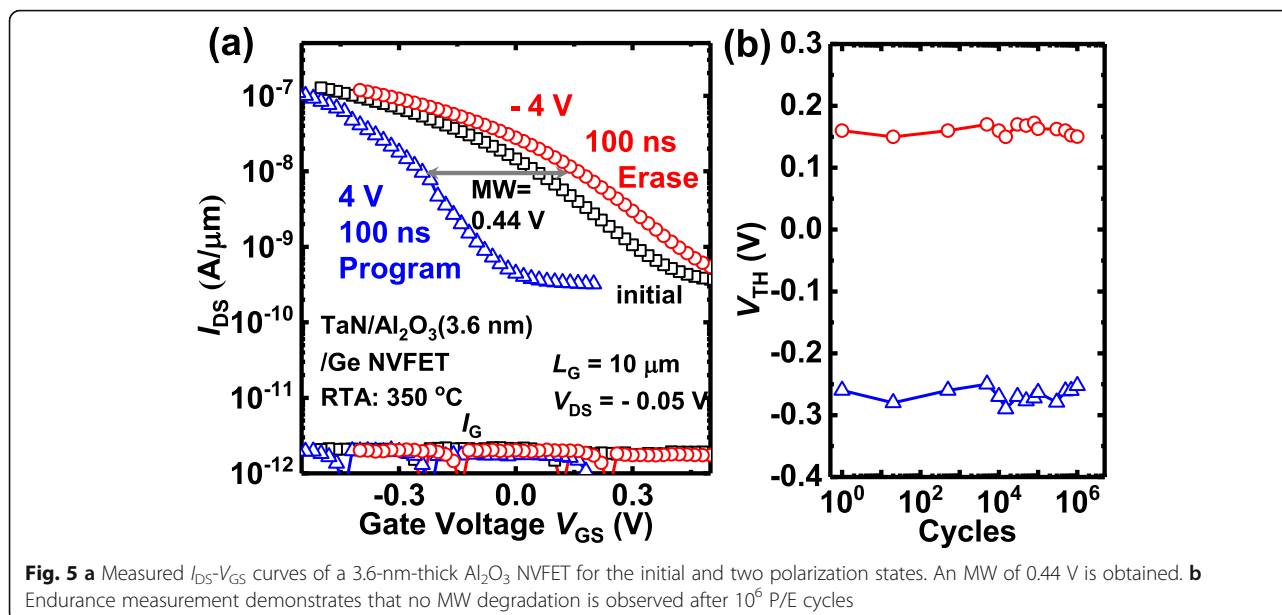
Fig. 5 a Measured I_{DS}-V_{GS} curves of a 3.6-nm-thick Al_2O_3 NVFET for the initial and two polarization states. An MW of 0.44 V is obtained. **b** Endurance measurement demonstrates that no MW degradation is observed after 10^6 P/E cycles

V_{TH}. The Al_2O_3 NVFET obtains an MW of 0.44 V, though amorphous Al_2O_3 film has smaller P_r than the reported doped HfO_2 films [5, 8]. It is noted that the high operating frequency up to 10 MHz of Al_2O_3 NVFET memory, which is indicative of that switchable P in Al_2O_3 originates from the migration of voltage-driven oxygen vacancy to form dipoles, not from defects charge trapping/detrapping. Alternating program and erase pulses were applied to the Al_2O_3 devices to further study the device endurance. Figure 5b shows the plots of V_{TH} vs. P/E cycle number, suggesting a stable MW can be maintained without a significant degradation over 10^6 P/E cycles for a 3.6-nm-thick Al_2O_3 NVFET.

Notably, the ferroelectric-like behavior observed in the amorphous Al_2O_3 devices can be extended to the universal amorphous oxides, e.g., hafnium oxide (HfO_2) and zirconium oxide (ZrO_2).

Conclusions

Stable ferroelectric-like behavior is first realized in capacitors with a thin amorphous Al_2O_3 insulator. Switchable P in amorphous Al_2O_3 capacitors is demonstrated by P-V loops and NVFET test. The ferroelectric-like behavior is proposed to be originating from the interface oxygen vacancies and ions dipoles. The 3.6-nm-thick Al_2O_3 NVFET achieves an MW of 0.44 V and over 10^6 cycle endurance under ±4 V at 100 ns P/E condition. All in all, this work opened a new world for amorphous oxide ferroelectric devices, which are promising for multi-gate (fin-shaped, nanowire, or nanosheet) NVFETs with potentially nano-scaled fin pitch in VLSI systems.

Abbreviations
Al_2O_3: Aluminum oxide; ALD: Atomic layer deposition; BF_2^+: Boron fluoride ion; E_c: Coercive electric field; Ge: Germanium; GeO_x: Germanium oxide; HRTEM: High-resolution transmission electron microscope; I_{DS}: Drain current; MOSFETs: Metal-oxide-semiconductor field-effect transistors; MW: Memory window; Ni: Nickel; NVFET: Non-volatile field-effect transistor; P_r: Remnant polarization; P_{sat}: Saturation polarization; RTA: Repaid thermal annealing; $TaAlO_x$: Tantalum aluminum oxide; t_{AlO}: Aluminum oxide thickness; TaN: Tantalum nitride; V_{GS}: Gate voltage; V_{TH}: Threshold voltage; XPS: X-ray photoelectron spectra

Authors' Contributions
YP carried out the experiments and drafted the manuscript. GQH, YP, and WWX designed the experiments. FNL, NZ, and CGD helped to measure the device. GQH, YL, ZF, and HD helped to revise the manuscript. YH supported the study. The authors read and approved the final manuscript.

Availability of Data and Materials
The datasets supporting the conclusions of this article are included in the article.

Competing Interests
The authors declare that they have no competing interests.

Author details
[1]State Key Discipline Laboratory of Wide Band Gap Semiconductor Technology, School of Microelectronics, Xidian University, Xi'an 710071, China. [2]Key Laboratory of Polar Materials and Devices, Ministry of Education, East China Normal University, Shanghai 200241, China. [3]Key Laboratory of Photoelectronic, Thin Film Devices and Technology of Nankai University, Tianjin 300071, China.

Peng *et al. Nanoscale Research Letters*   (2020) 15:134

Page 6 of 6

References

1. J. F. Scott, Nanostructures: synthesis, functional properties and applications. (Springer, Dordrecht, 2003), 584-600
2. Liu Y, Zhang Y, Chow M-J, Chen QN, Li J (2012) Biological ferroelectricity uncovered in aortic walls by piezoresponse force microscopy. Phys Rev Lett 108:078103
3. Varghese J, Barth S, Keeney L, Whatmore RW, Holmes JD (2012) Nanoscale ferroelectric and piezoelectric properties of Sb_2S_3 nanowire arrays. Nano Lett 12:868–872
4. Mukherjee S, Roy A, Auluck S, Prasad R, Gupta R, Garg A (2013) Room temperature nanoscale ferroelectricity in magnetoelectric epitaxial thin films. Phys Rev Lett 111:087601
5. Böscke TS, Müller J, Bräuhaus D, Schröder U, Böttger U (2011) Ferroelectricity in hafnium oxide thin films. Appl Phys Lett 99:102903
6. Lang SB, Tofail SAM, Kholkin AL, Wojtaś M, Gregor M, Gandhi AA, Wang Y, Bauer S, Krause M, Plecenik A (2013) Ferroelectric polarization in nanocrystalline hydroxyapatite thin films on silicon. Sci Report 3:2215
7. Bark C, Sharma P, Wang Y, Baek SH, Lee S, Ryu S, Folkman C, Paüdel TR, Kumar A, Kalinin SV (2012) Switchable induced polarization in $LaAlO_3/SrTiO_3$ heterostructures. Nano Lett 12:1765–1771
8. J. Müller T. S. Böscke, S. Muller, E. Yurchuk, P. Polakowski, J. Paul, D. Martin, T. Schenk, K. Khullar, A. Kersch, W. Weinreich, S. Riedel, K. Seidel, A. Kumar, T. M. Arruda, S. V. Kalinin, T. Schlösser, R. Boschke, R. van Bentum, U. Schröder, T. Mikolajick (2013) Ferroelectric hafnium oxide: a CMOS-compatible and highly scalable approach to future ferroelectric memories, in IEDM Tech Dig. , 10.8.1-10.8.4.
9. M. D. Glinchuk, A. N. Morozovska, A. Lukowiak, W. Stręk, M. V. Silibin, D. V. Karpinsky, Y. Kim, S. V. Kalinin (2020) Possible electrochemical origin of ferroelectricity in HfO2 thin films, Journal of Alloys and Compounds, Available online, 153628.
10. Daus A, Lenarczyk P, Petti L, Münzenrieder N, Knobelspies S, Cantarella G, Vogt C, Salvatore GA, Luisier M, Tröster G (2017) Ferroelectric-like charge trapping thin-film transistors and their evaluation as memories and synaptic devices. Adv Electron Mater 3:1700309
11. W. Chung, M. Si, and P. D. Ye (2017) Hysteresis-free negative capacitance germanium CMOS FinFETs with bi-directional sub-60 mV/dec, in IEDM Tech. Dig., 365-368.
12. Smith SW, Kitahara AR, Rodriguez MA, Henry MD, Brumbach MT, Ihlefeld JF (2017) Pyroelectric response in crystalline hafnium zirconium oxide ($Hf_{1-x}Zr_xO_2$) thin films. Appl Phys Lett 110:072901
13. Dong R, Xiang WF, Lee DS, Oh SJ, Seong DJ, Heo SH, Choi FJ, Kwon MJ, Chang M, Jo M, Hasan M, Hwang H (2007) Improvement of reproducible hysteresis and resistive switching in metal-$La_{0.7}Ca_{0.3}MbO_3$-metal heterostructures by oxygen annealing. Appl Phy Lett 90:182118
14. Starschich S, Menzel S, Böttger U (2016) Evidence for oxygen vacancies movement during wake-up in ferroelectric hafnium oxide. Appl Phy Lett. 108:032903
15. G. Bersuker, D. C. Gilmer, D. Veksler, J. Yum, H. Park, S. Lian, L. Vandelli, A. Padovani, L. Larcher, K. Mckenna, A. Shluger, V. Iglesias, M. Porti, M. Nafría, W. Taylor, P. D. Kirsch, R. Jammy (2010) Metal oxide RRAM switching mechanism based on conductive filament microscopic properties, in IEDM Tech Dig, 19.6.1-19.6.4.
16. N. Xu, B. Gao, L. F. Liu, B. Sun, X. Y. Liu, R. Q. Han, J. F. Kang, B. Yu (2008) A unified physical model of switching behavior in oxide-based RRAM, in VLSI Tech. Symp. 100-101.
17. Tsai T-L, Ho T-H, Tseng T-Y (2015) Unipolar resistive switching behaviors and mechanisms in an annealed $Ni/ZrO_2/TaN$ memory device. J Phys D Appl Phys 48:035108

Publisher's Note

Springer Nature remains neutral with regard to jurisdictional claims in published maps and institutional affiliations.